

# Millimeter-Wave Reflectionless Filters Using Advanced Thin-Film Fabrication

Matthew A. Morgan, *Senior Member, IEEE*, Seng Loo, Tod A. Boyd, and Miho Hunter

**Abstract**—We report on the development of millimeter-wave, lumped-element reflectionless filters using an advanced thin-film fabrication process. Based on previously demonstrated circuit topologies capable of achieving  $50\Omega$  impedance match at all frequencies, these circuits have been implemented at higher frequencies than ever before by leveraging a thin-film process with better than  $2\ \mu\text{m}$  feature size and integrated elements such as SiN Metal-Insulator-Metal (MIM) capacitors, bridges, and TaN Thin-Film Resistors (TFRs).

**Index Terms**—filters, thin film circuits, reflectionless filters, absorptive filters

## I. INTRODUCTION

THE concept of an absorptive filter dates back at least to the 1920's, nearly a century ago, with the work of Zobel [1] and Bode [2], when they were called *constant-resistance networks* and were based on image-impedance principles, bridged-tee's, and cascaded, first and second-order lattice sections. However, the practical limitations on the performance and realizability of such designs precluded them from becoming widely adopted. However, interest in absorptive, or *reflectionless* filters has experienced a resurgence in recent years, owing initially to the discovery of lumped-element topologies that could theoretically achieve perfect impedance match at both ports and at all frequencies from DC to infinity, with no added passband loss [3], [4]. At first limited to a single response type, that of a third-order Chebyshev type II filter, a broader theory of symmetric and self-dual circuit topologies was built upon this foundation until it was eventually found that any transfer function whatsoever that was realizable using lumped elements could likewise be implemented in reflectionless form [5]–[12].

Seeing the advantages of a filter that absorbs stop-band energy instead of reflecting it, many researchers began searching for ways to duplicate these results using other circuit elements, such as transmission lines [13]–[19], coaxial resonators [20], [21], and Surface Acoustic Wave (SAW) resonators [22], as well as other methodologies, most importantly coupling-routing diagrams [20]–[27]. These often resulted in somewhat larger filters for a given frequency with limited absorption

Manuscript received 6/20/2023

M. Morgan and T. Boyd are with the Central Development Laboratory, National Radio Astronomy Observatory, Charlottesville, VA, 22903 USA (e-mail: matt.morgan@nrao.edu). The National Radio Astronomy Observatory is a facility of the National Science Foundation operated under cooperative agreement by Associated Universities, Inc.

Seng Loo and Miho Hunter are with Anritsu Company, Morgan Hill, CA, 95037 USA.

TABLE I  
CHEBYSHEV PROTOTYPE PARAMETERS FOR LIMITING RIPPLE FACTORS

$N$	$\epsilon$	$g_1$	$g_2$	$g_3$	$g_4$	$g_5$	$g_6$	$g_7$
5	0.2164	1.337	1.337	2.164	1.337	1.337		
7	0.2187	1.377	1.377	2.280	1.498	2.280	1.377	1.377

bandwidth (theoretically as well as practically), and/or with stop-band impedance-matching only at a single port. For this work, we will concentrate on lumped-element designs, as these are generally capable of the broadest absorption bandwidth in the most compact form.

Originally fabricated at relatively low frequencies using discrete surface-mount elements, these topologies were eventually implemented in the microwave regime using an Integrated Passive Device (IPD) fabrication process on GaAs wafers [28]. Thus, having been reduced to practice in a form suitable for cost-effective mass manufacturing, these devices have become adopted by industry as the preferred solution in a number of commercial applications [29]–[32]. However, the difficulty of realizing good-quality lumped-elements at short wavelengths has limited their cutoff frequencies primarily to the cm-wave range (though passband and absorption bandwidths often extend much higher).

With the advent of sophisticated thin-film fabrication that combines integrated circuit elements (MIM caps, bridges, and TFRs) with photolithography having even better resolution than is generally achievable with commercial III-V semiconductor processes, we are now prepared to implement lumped-element circuits of this kind for the first time in the millimeter-wave regime. This capability is demonstrated by the development of two prototypes: a fifth-order Chebyshev type II low-pass filter, and a seventh-order Chebyshev type II high-pass filter.

## II. SCHEMATIC FILTER DESIGN

Circuit diagrams of the two prototype filters reported in this paper are shown in Fig. 1. Fig. 1(a) is a fifth-order low-pass filter, while Fig. 1(b) is a seventh-order, high-pass filter. Both are Chebyshev Type II designs, having equal stop-band ripple, and are theoretically reflectionless at both ports and at all frequencies.

The prototype parameter values used for these designs is given in Table I. The ripple factor has been selected to achieve the maximum theoretical stop-band rejection for these topologies (without requiring transformers, which are

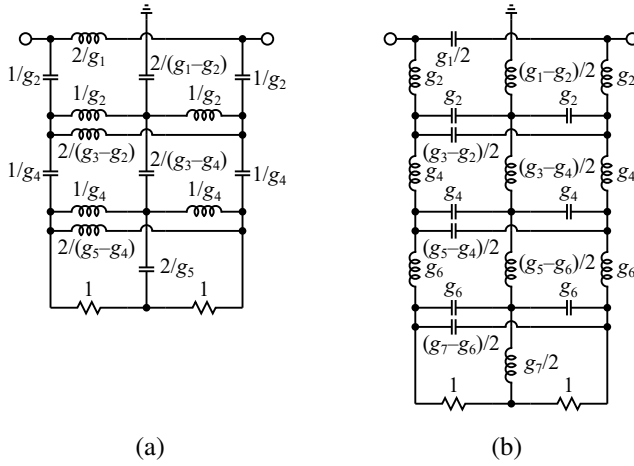


Fig. 1. (a) Fifth-order low-pass and (b) seventh-order high-pass filters implemented in advanced thin-film technology for this paper.

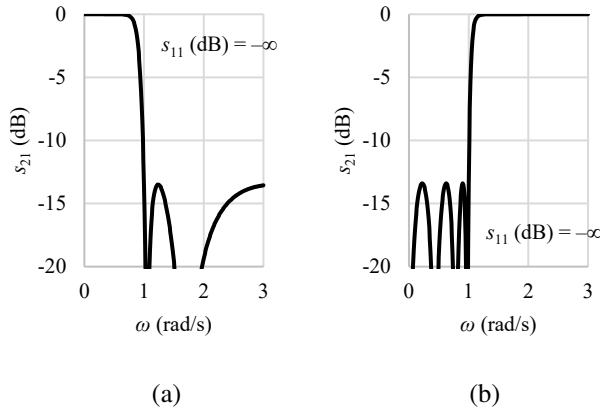


Fig. 2. Ideal, normalized frequency response of (a) fifth-order low-pass and (b) seventh-order high-pass reflectionless filters.

difficult to implement at such high frequencies in planar circuit technology). That is, the ripple factor,  $\varepsilon$ , is given by

$$\varepsilon = \sqrt{e^{4 \tanh^{-1}(e^{-\beta})} - 1} \approx \begin{cases} 0.2164 & N = 5 \\ 0.2187 & N = 7 \end{cases} \quad (1)$$

where

$$\beta = 2N \sinh^{-1} \left( \sqrt{\frac{1}{2} \sin \left( \frac{\pi}{N} \right) \tan \left( \frac{\pi}{N} \right)} \right) \quad (2)$$

and  $N$  is the order of the filter [5], [6]. Consequently, the stop-band rejection here is theoretically limited to about 13.5 dB, as shown by their ideal, normalized frequency responses in Fig. 2. It has become common practice to cascade multiple stages of such designs to achieve the level of stop-band attenuation desired for a given application, however single-stage designs are sufficient for the present proof-of-concept.

### III. PHYSICAL ELEMENT DESIGN

Note that by selecting the minimum ripple factors, the first and last two elements in each row of Table I are identical. This means that certain elements in the schematics of Fig. 1 shall vanish in the final layout—e.g. the capacitor  $2/(g_1 - g_2)$

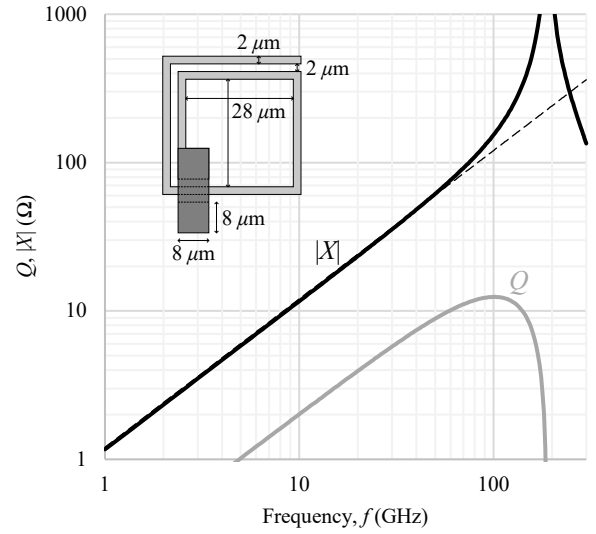


Fig. 3. Inductor layout (inset), simulated reactance and quality factor (solid lines), and theoretical reactance of an ideal 192 pH inductor (dashed line).

and the inductor  $2/(g_5 - g_4)$  in Fig. 1(a). Others will be split in two in favor of layout symmetry—for example, the series inductor having value  $2/g_1$  will be implemented with two series inductors in the physical filter, mirrored, having normalized value  $1/g_1$  each.

We selected a cutoff frequency of 60 GHz for both designs. This required capacitors ranging from 40–120 pF. These were implemented as Metal-Insulator-Metal (MIM) capacitors with a Silicon Nitride (SiN) dielectric. The inductors needed ranged from 99–199 pH. They were implemented as planar spiral coils having 1.5 turns each in the first metal layer. The fine lithography of the process made it possible to use trace widths and spacings of  $2 \mu\text{m}$  each. The internal node of the coil was brought out using a dielectric bridge (the same SiN dielectric used for the capacitors). This extra parasitic capacitance at the bridge was accepted as a compromise between the simplicity of the fabrication process and the self-resonance of the inductor. A typical inductor layout for these filters is shown in Fig. 3, as the inset on a graph showing the simulated reactance and quality factor as a function of frequency. It shows that a linear reactance curve is achieved from the lowest frequencies up to around W-band, eventually reaching a self-resonance at nearly 200 GHz. The peak  $Q$ , modelled at around 100 GHz, was about 12.

### IV. THIN FILM FABRICATION PROCESS

The thin-film circuits were fabricated on a quartz substrate, specifically Corning Fused Silica 7980. Resistors were fabricated using Tantalum Nitride (TaN) film with a target sheet resistance of  $50 \Omega/\text{sq}$ . The reflectionless filters are relatively insensitive to resistor value, so a tolerance of  $\pm 10\%$  was accepted for this film. The first metalization comprised TiW/Au, plated up to a final thickness of  $1.25 \mu\text{m}$ . Silicon Nitride (SiN) was then deposited to a target thickness of  $1 \mu\text{m}$ , giving an expected capacitance density of  $0.062 \text{ fF}/\mu\text{m}^2$ . The second

metal layer again used TiW/Au, plated up to a thickness of  $2.5 \mu\text{m}$ .

The final metal stack was therefore TaN/TiW/Au ( $1.25 \mu\text{m}$ )/SiN ( $1 \mu\text{m}$ )/TiW/Au ( $2.5 \mu\text{m}$ ). An MRC 943 Series Sputter and TemesCal VES-2550 E-beam Evaporator are used for the metal deposition processes. Photolithography imaging was carried out using positive tone resists and a Canon FPA2000-il 5 X Stepper. Silicon Nitride deposition was carried out using a Novellus Concept One PECVD tool. Finally, gold electroplating utilized a Gold Sulfite plating system from Tanaka.

The potential for capacitor shorts was considered a risk for this fabrication process. The initial attempt utilized a much thinner first metalization layer of  $0.4 \mu\text{m}$ , in order to keep the the surface as smooth as possible for the subsequent Silicon Nitride deposition. While the capacitor yield was excellent (no shorts were discovered), the ohmic losses of the metal traces was unacceptably high. Having greater confidence then in the capacitor process, a second run was initiated having the thicker metalization stack described above.

After all other processing steps were completed, the wafer was thinned to a final thickness of  $125 \mu\text{m}$ , and diced into individual die.

## V. MEASUREMENTS

Both circuits were fabricated on a 100-mm diameter quartz wafer, containing over 14,000 chips, or 7,000 of each design. Microphotographs of the two circuits are shown in Fig. 4. The chips were tested by wafer probe using a Keysight N5291A-201 Vector Network Analyzer (VNA) capable of measuring two-port scattering parameters from 900 Hz–120 GHz in a single sweep. The results are plotted in Fig. 5. The measured response curves for both filters, plotted in solid lines, were shifted upward in frequency 5-10% compared to the initial simulations. This was attributed to the SiN capacitor dielectric, initially assumed to have a dielectric constant of  $\epsilon_r = 7$ . For the simulations plotted in Fig. 5 (dashed lines) the dielectric constant was decreased to account for this error, but still within the acceptable range reported in literature [33]. This brought the measured and simulated results within good agreement across the whole frequency range. This also partly accounted for the increased reflection coefficients in the stop-band of the low-pass filter and the transition-band of the high-pass filter.

DC resistance measurements were additionally performed at sites across the entire wafer to verify trace conductivity, and to test for shorted or leaking capacitors, which as discussed previously were considered a technical risk for this fabrication. One low-pass filter in each of 82 reticles was probe-tested for DC isolation between one of the port signal pads and ground. This is nominally expected to be an open circuit. However, if either of the first two capacitors, labeled  $1/g_2$  in Fig. 2(a), is shorted or leaky, then a finite resistance will be measured (recall that the grounded capacitor  $2/(g_1 - g_2)$  vanishes since  $g_1 = g_2$ ).

The leakage test results are summarized in the wafer map of Fig. 6 (“0L” means no measurable leakage was detected). Out of 82 reticles, 13 showed signs of some leakage, all clustered

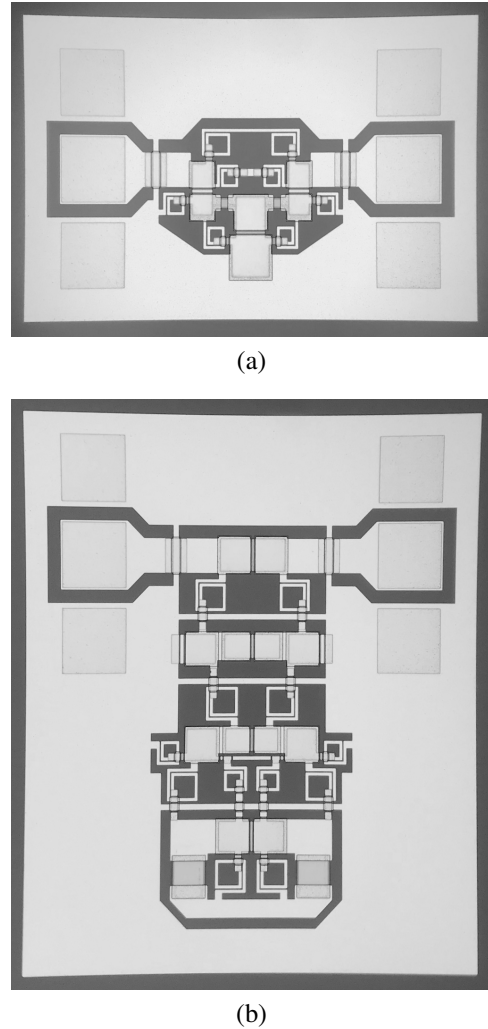


Fig. 4. Microphotographs of thin-film, reflectionless filters. (a) Low-pass filter measuring  $600 \mu\text{m} \times 400 \mu\text{m}$ . (b) High-pass filter measuring  $600 \mu\text{m} \times 700 \mu\text{m}$ . The substrate is  $125\text{-}\mu\text{m}$  thick quartz.

around the outer edge of the wafer. We thus estimate the global capacitor yield as  $Y_C = \sqrt{69/82} \approx 92\%$  (the square root is used since two capacitors must both be good for the isolation test to pass). Closer to the center, presumably the yield is much higher (none of the devices tested in the interior, whether at DC or RF, was found to be defective).

## VI. CONCLUSION

This paper has presented reflectionless low-pass and high-pass filters on quartz in the millimeter-wave band. Each has a cutoff frequency at approximately 60 GHz. Furthermore, the absorptive stop-band of the low-pass filter and pass-band of the high-pass filter extend up to 120 GHz, the limit of our measurement equipment. These represent the highest operating frequencies ever reported for reflectionless filters, and a landmark achievement for strictly lumped-element-based designs.

This performance was made possible by an advanced thin-film fabrication process capable of extraordinary lithographic resolution, down to  $2 \mu\text{m}$ , combined with integrated circuit elements like MIM caps, bridges, and thin-film resistors. The

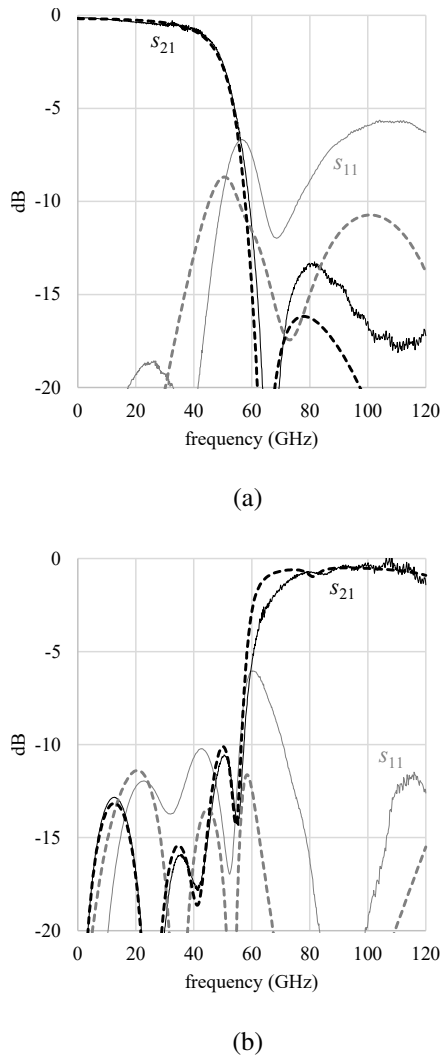


Fig. 5. Measured (solid lines) and simulated (dashed lines) s-parameters for (a) low-pass, and (b) high-pass reflectionless filters. The SiN dielectric was adjusted to account for an apparent shift in frequency between the measurements and the initial simulations.

process shows high yield, suitable for mass manufacturing and commercialization.

The advantages of these designs and of this fabrication technology are strikingly illustrated by the plot in Fig. 7, which compares this work to numerous others in the references in terms of compactness (on the vertical axis) versus frequency (on the horizontal). Note that both scales are logarithmic, spanning five orders of magnitude in frequency and three orders of magnitude in physical size.

It is interesting to see how well the different approaches to reflectionless filters naturally segregate themselves into clusters on such a plot. Lumped-element designs using surface-mount (SMT) components appear in the upper left as relatively large circuits at low frequency. In contrast, filters on microwave laminates or soft board materials, almost universally implemented using distributed elements such as transmission lines [13]–[19] or substrate-integrated resonators [20], [21], increase the frequency without any real reduction in size, thus grouping together in the upper-right corner.

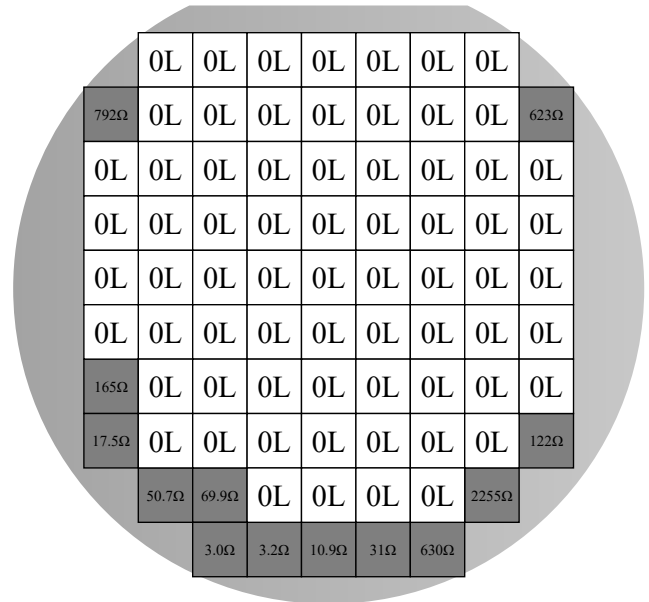


Fig. 6. DC isolation between the low-pass signal port pad and ground. Out of 82 sites measured, 13 showed evidence of leakage in the capacitors.

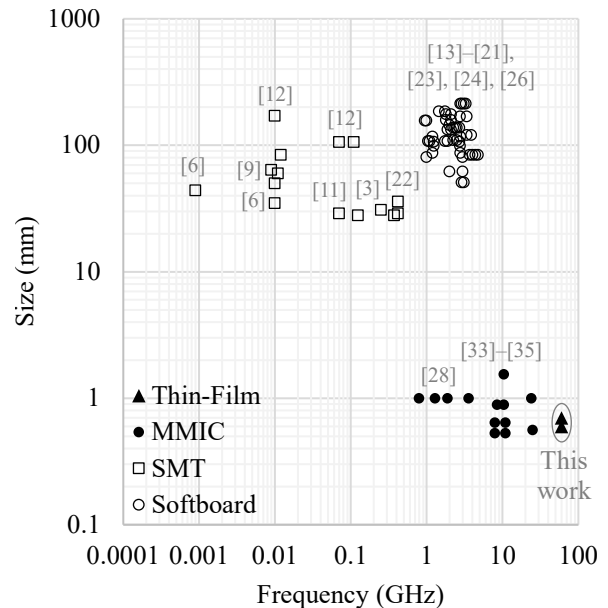


Fig. 7. Comparison of this work with other approaches to reflectionless filters in terms of size (the largest linear dimension) and cutoff frequency. All cutoff corners for band-pass, band-stop, and multiple-band filters are shown. Bond pads are included in the circuit dimensions.

The smallest and most high-frequency designs have all, until now, been implemented using MMIC fabrication, usually lumped-element, on either a GaAs IPD or Silicon CMOS wafer. The two filters reported here, using a thin-film process on quartz, appear in the extreme bottom right corner of the plot, achieving the highest frequencies in form-factors that are amongst the smallest ever reported.

#### ACKNOWLEDGMENT

The authors with NRAO would like to thank their commercial partner, Mini-Circuits Inc., for their continued support of the development and application of reflectionless filter technology.

#### REFERENCES

- [1] O. Zobel, "Distortion correction in electrical circuits with constant resistance recurrent networks," *Bell System Technical Journal*, Vol. 7, 1928.
- [2] H. Bode, *Network Analysis and Feedback Amplifier Design*. New York: Van Nostrand, 1945.
- [3] M. Morgan and T. Boyd, "Theoretical and experimental study of a new class of reflectionless filter," *IEEE Trans. Microwave Theory Tech.*, vol. 59, no. 5, pp. 1214–1221, May 2011.
- [4] M. Morgan, "Reflectionless filters," U.S. Patent 8 392 495, March 5, 2013.
- [5] M. Morgan, *Reflectionless Filters*. Norwood, MA: Artech House, 2017.
- [6] M. Morgan, W. Groves, and T. Boyd, "Reflectionless filter topologies supporting arbitrary low-pass ladder prototypes," *IEEE Transactions on Circuits and Systems I*, vol. 66, no. 2, pp. 594–604, February 2019.
- [7] M. Morgan, "Optimal response reflectionless filters," U.S. Patent 10 263 592, April 16, 2019.
- [8] M. Morgan, "Deep rejection reflectionless filters," U.S. Patent No. 10 530 321, January 7, 2020.
- [9] A. Guilabert, M. Morgan, and T. Boyd, "Reflectionless filters for generalized elliptic transmission functions," *IEEE Transactions on Circuits and Systems I*, vol. 66, no. 12, pp. 4606–4618, December 2019.
- [10] M. Khalaj-Amirhosseini and A. Khalaj-Amirhosseini, "Reflectionless filters with arbitrary transfer functions," *Journal of Telecommunication*, vol. 34, no. 2, pp. 1–3, Oct. 2016.
- [11] M. Khalaj-Amirhosseini and M. M. Taskhiri, "Twofold reflectionless filters of inverse-chebyshev response with arbitrary attenuation," *IEEE Trans. Microwave Theory Tech.*, vol. 65, no. 11, pp. 4616–4620, November 2017.
- [12] J. Lee, B. Lee, S. Nam, and J. Lee, "Rigorous design method for symmetric reflectionless filters with arbitrary prescribed transmission response," *IEEE Trans. Microwave Theory Tech.*, vol. 68, no. 6, June 2020.
- [13] D. Psychogiou and R. Gomez-Garcia, "Tunable reflectionless microstrip bandpass filters," *IEEE Radio Wireless Symposium*, January 2018.
- [14] R. Gomez-Garcia, J. M. Munoz-Ferreras, Wenjie Feng, and D. Psychogiou, "Balanced symmetrical quasi-reflectionless single- and dual-band bandpass filters," *IEEE Microwave and Wireless Comp. Lett.*, vol. 28, no. 9, pp. 798–800, September 2018.
- [15] L. Yang, R. Gomez-Garcia, J. M. Munoz-Ferreras, R. Zhang, D. Peroulis, and L. Zhu, "Multilayered reflectionless wideband bandpass filters with shunt/in-series resistively terminated microstrip lines," *IEEE Trans. Microwave Theory Tech.*, vol. 68, no. 3, pp. 877–893, March 2020.
- [16] R. Gomez-Garcia, L. Yang, and J. M. Munoz-Ferreras, "Low-reflection signal-interference single- and multipassband filters with shunted lossy stubs," *IEEE Microwave and Wireless Comp. Lett.*, vol. 30, no. 4, pp. 355–358, April 2020.
- [17] X. Wu, Y. Li, and X. Liu, "Quasi-reflectionless microstrip bandpass filters with improved passband flatness and out-of-band rejection," *IEEE Access*, vol. 8, August 2020.
- [18] M. Fan, K. Song, L. Yang, and R. Gomez-Garcia, "Balanced-circuit-based dual-band bandpass filter with symmetrical reflectionless behavior," *IEEE Radio Wireless Symposium*, January 2021.
- [19] J. Lee and J. Lee, "Transmission-line absorptive bandpass filters with wide passband: synthesis and design," *IEEE Trans. Microwave Theory Tech.*, vol. 69, no. 12, pp. 5371–5380, December 2021.
- [20] D. Psychogiou, and R. Gomez-Garcia, "Quasi-absorptive substrate-integrated bandpass filters using capacitively-loaded coaxial resonators," *IEEE MTT-S Intl. Microwave Symp.*, August 2020.
- [21] K. Zhao, R. Gomez-Garcia, and D. Psychogiou, "Tunable quasi-reflectionless bandpass filters using substrate integrated coaxial resonators," *IEEE Trans. Circuits and Systems II*, vol. 69, no. 2, pp. 379–383, February 2022.
- [22] D. Psychogiou, and R. Gomez-Garcia, "Symmetrical quasi-reflectionless SAW-based bandpass filters with tunable bandwidth", *IEEE Microwave and Wireless Comp. Lett.*, vol. 29, no. 7, pp. 447–449, July 2019.
- [23] R. Gomez-Garcia, J. M. Munoz-Ferreras, and D. Psychogiou, "Symmetrical quasi-reflectionless BSFs," *IEEE Microwave and Wireless Comp. Lett.*, vol. 28, no. 4, pp. 302–304, April 2018.
- [24] R. Gomez-Garcia, J. M. Munoz-Ferreras, and D. Psychogiou, "Split-type input-reflectionless multiband filters," *IEEE Microwave and Wireless Comp. Lett.*, vol. 28, no. 11, pp. 981–983, November 2018.
- [25] R. Gomez-Garcia, J. M. Munoz-Ferreras, and D. Psychogiou, "Symmetrical quasi-absorptive RF bandpass filters," *IEEE Trans. Microwave Theory Tech.*, vol. 67, no. 4, pp. 1472–1482, April 2019.
- [26] R. Gomez-Garcia, J. M. Munoz-Ferreras, and D. Psychogiou, "High-order input-reflectionless bandpass/bandstop filters and multiplexers," *IEEE Trans. Microwave Theory Tech.*, vol. 67, no. 9, pp. 3683–3695, September 2019.
- [27] R. Gomez-Garcia, D. Psychogiou, J. M. Munoz-Ferreras, and L. Yang, "Avoiding RF isolators: reflectionless microwave bandpass filtering components for advanced RF front ends," *IEEE Microwave Magazine*, vol. 21, no. 12, November 2020.
- [28] M. Morgan, and T. Boyd, "Reflectionless filter structures," *IEEE Trans. Microwave Theory Tech.*, vol. 63, no. 4, April 2015.
- [29] Mini-Circuits Inc. (2015). *Pairing Mixers With Reflectionless Filters to Improve System Performance*. [Online]. Available: <https://www.minicircuits.com/app/AN75-007.pdf>
- [30] Mini-Circuits Inc. (2015). *Advantages of Cascading Reflectionless Filters*. [Online]. Available: <https://www.minicircuits.com/app/AN75-008.pdf>
- [31] R. Setty, B. Kaplan, M. Morgan, and T. Boyd, "Combining MMIC reflectionless filters to create UWB bandpass filters," *Microwave Journal*, vol. 61, no. 3, March 2018.
- [32] R. Shrotriya and M. Morgan, "Filtering without reflections: flattening multiplier chain conversion efficiency & more," *Microwave Journal*, vol. 62, no. 9, September 2019.
- [33] A. Piccirillo and A. L. Gobbi, "Physical-electrical properties of silicon nitride deposited by PECVD on III-V Semiconductors," *Journal of the Electrochemical Society*, vol. 137, no. 12, pp. 3910–3917, December 1990.
- [34] D. Simpson and D. Psychogiou, "X-band quasi-reflectionless MMIC bandpass filters with minimum number of components," *IEEE Trans. Elec. Dev.*, vol. 68, no. 9, pp. 4329–4334, September 2021.
- [35] Z. Ge, L. Chen, L. Yang, R. Gomez-Garcia, and X. Zhu, "On-chip millimeter-wave integrated absorptive bandstop filter in (Bi)-CMOS technology," *IEEE Electron Device Lett.*, vol. 42, no. 1, pp. 114–117, January 2021.
- [36] K. Zhao and D. Psychogiou, "X-band MMIC-based tunable quasi-absorptive bandstop filter," *IEEE Microwave and Wireless Tech. Lett.*, vol. 33, no. 4, pp. 391–394, April 2023.



**Matthew A. Morgan** (M'99–SM'17) received his B.S. in electrical engineering from the University of Virginia in 1999, and his M.S. and Ph.D. from the California Institute of Technology in 2001 and 2003, respectively.

During the summers of 1996 through 1998, he worked for Lockheed Martin Federal Systems in Manassas, VA, as an Associate Programmer, where he wrote code for acoustic signal processing, mathematical modeling, data simulation, and system performance monitoring. In 1999, he became an affiliate

of NASA's Jet Propulsion Laboratory in Pasadena, CA. There, he conducted research in the development of Monolithic Millimeter-wave Integrated Circuits (MMICs) and MMIC-based receiver components for atmospheric radiometers, laboratory instrumentation, and the deep-space communication network. In 2003, he joined the Central Development Lab (CDL) of the National Radio Astronomy Observatory (NRAO) in Charlottesville, VA, where he now holds the position of Scientist/Research Engineer. He is currently the head of the CDL's Integrated Receiver Development program, and is involved in the design and development of low-noise receivers, components, and novel concepts for radio astronomy instrumentation in the cm-wave, mm-wave, and submm-wave frequency ranges. He has authored over 60 papers and holds twenty patents in the areas of MMIC design, millimeter-wave system integration, and high-frequency packaging techniques. He is the author of *Reflectionless Filters* (Norwood, MA: Artech House, 2017).

Dr. Morgan is a member of the International Union of Radio Science (URSI), Commission J: Radio Astronomy. He received a Topic Editor's Special Mention in the IEEE THz Transactions Best Paper competition and the Harold A. Wheeler Applications Paper Award in 2015.



**Seng Loo** received his BS in Chemistry from the University of Windsor, in Ontario, Canada, and his Ph.D from Stanford University in 1991.

From 1991 through 1993 he worked as a Postdoc at the California Institute of Technology, where he carried out basic research in yeast genetics. Since 1994, he has been working in various industrial companies, including Seagate, Hyundai Electronics and Watkins-Johnson Company.

Since 2006, he has been the Fab Manager, and then Senior Business Unit Manager for the Anritsu

Microelectronics Fabrication Center. In this capacity, he is tasked with leading and growing the manufacturing capabilities of the Anritsu fab.



**Tod A. Boyd** was born in Steubenville, Ohio, in 1962. He received the A.S.E.E. degree from the Electronic Technology Institute, Cleveland, Ohio, in 1983. From 1983 to 1985, he was with Hostel Electronics in Steubenville, Ohio. In 1985, he joined Northrop Corporation's Electronic Countermeasures Division, in Buffalo Grove, Ill., specialized in supporting the B-1B Lancer (secret clearance.) In 1990, he joined Interferometrics, Inc., Vienna, Va., where he constructed VLBA tape recorders for the international Radio Astronomy community.

Since 1996, he has been with the National Radio Astronomy Observatory's Central Development Lab, Charlottesville, VA, where he initially assisted with the construction of cooled InP HFET amplifiers for the NASA's Wilkinson Microwave Anisotropy Probe (WMAP) mission. Presently as a Technical Specialist IV he provides technical support for the advanced receiver R&D initiatives. His responsibilities also include constructing low noise amplifiers for the Enhanced VLA and the Atacama Large Millimeter/sub-millimeter Array (ALMA) projects.



**Miho Hunter** joined Anritsu Company in 2009 as a Process Development Engineer, supporting the Microelectronics Fabrication Center. In 2019, she advanced to the role of Operations and Process Engineering Manager, assuming responsibility for the process engineering group tasked with designing and integrating thin film fabrication processes. Prior to joining Anritsu, Miho honed her expertise at Samsung Austin Semiconductor, specializing in the process architecture of memory devices. She holds a Master of Science degree from Stanford University.